Mixed Poiseuille-Knudsen flow model for Gas Liquid Displacement porometry data treatment

Md. Akhtarul Islam[1,*], Mohammad Shahedul Hossain[1], Carmen Garcia-Payo[2], Mohamed Khayet[3], Mathias Ulbricht[4,*]

[1] Department of Chemical Engineering and Polymer Science, Shahjalal University of Science and Technology (SUST), Sylhet-3114, Bangladesh.

*Email: mislam@sust.edu

[2] Department of Structure of Matter, Thermal Physics and Electronics, Faculty of Physics, University Complutense of Madrid, Av. Complutense s/n, 28040 Madrid, Spain.

[3] Madrid Institute of Advanced Studies of Water (IMDEA Water Institute), Av. Punto Com nº 2, 28805 Alcalá de Henares, Madrid (Spain)

[4] Lehrstuhl für Technische Chemie II, Universität Duisburg-Essen, D-45117 Essen, Germany.

* Email: mathias.ulbricht@uni-essen.de

Abstract

A comprehensive methodology has been developed for treating Gas Liquid Displacement (GLD) porometry data with a flow model called Weber model (WM) describing mixed Poiseuille-Knudsen flow regime. The model has been applied in two options: i) considering that the gas viscosity in porometry experiments is the same as that available in reference books for Poiseuille flow regime and ii) equating the expression for Darcy coefficient in gas flow to that obtained in additional liquid permeability experiments and thus leaving the gas viscosity to be an adaptable

parameter. In the analysis of GLD porometry data for a range of different microfiltration membranes, it is found that with the WM in both options identical relative pore-number distribution is estimated; and this distribution satisfactorily reproduces both dry and wet flow data from the GLD experiments. The absolute pore-number distributions obtained by the two options are quite similar, but differ in the absolute value of the pore numbers. The pore-number distribution obtained by the second option describes the liquid permeability well, while the first option fails. The WM as a method of GLD porometry data treatment is quite similar to the earlier introduced variable viscosity Poiseuille model (VVPM), and the variable viscosity from the latter model appears to be a combined effect of an uncertainty about actual gas viscosity and the contribution of Knudsen flow. It is concluded that a standard test method for determining pore-size distribution by GLD porometry must include prediction or description of liquid permeability of the membrane. Then, any acceptable gas flow model with adjusted Darcy coefficient obtained from liquid permeability experiment will be suitable for advanced GLD porometry data treatment, beyond the methods typically implemented in gas flow-based porometers, currently used in academia and industry.

Keywords: mixed Poiseuille-Knudsen flow; Weber model; pore-size distribution; microfiltration membrane; Gas-Liquid-Displacement porometry; Darcy coefficient for gas flow.

1. Introduction

Step by step opening of pores of different sizes, and simultaneously following the gradual increment in fluid flow through a filtration medium has become very appealing to investigators as a method of determining the pore-size distribution of filtration membranes since the pioneering theoretical work of Erbe [1], combining Young-Laplace equation for pore size estimation and Hagen-Poiseuille equation for fluid flow. Using this method, the automated porometer, namely "Coulter Porometer", for characterizing the pore-size distribution of microfiltration membranes emerged in the market in the 1980s [2]. Since then this technique has been used for characterizing many commercial membranes [3,4,5] and has been honored with the status of recommended standard [6,7]. However, there remains a fine difference between the proposed methodology of Erbe and the principle of operation of the porometer. Erbe worked out the methodology based on the liquid-liquid displacement concept [1], but the Coulter porometer used gas-liquid displacement (GLD) method. While the liquid flow through capillaries is well-described by Hagen-Poiseuille equation, the law governing gas flow through capillaries under the conditions of porometry data acquisition seems not well-formulated. For this reason, the software supplied with commercial porometers available in the market practically applies only Young-Laplace equation for detecting pore diameters, and treats the GLD porometry flow data phenomenologically relating the portion of gas flow to a given range of pore-diameter. Thus, the use of a flux equation is avoided, but as a consequence, no information is obtained about the pore number density distribution, pore uniformity or tortuosity of the investigated membrane and its probable liquid permeability.

Recently, a thorough analysis of GLD porometry data combining the Young-Laplace equation with several flux model equations has been made [8,9]. Two groups of flux models were considered:

i) ones with constant gas viscosity concept, that include conventional Poiseuille model (PM), Klinkenberg model (KM) and Forchheimer model (FM) and

ii) ones with variable viscosity concept, that include two newly proposed modified Poiseuille models (variable viscosity Poiseuille model (VVPM) and unified Poiseuille model (UPM)).

Both modified Poiseuille models, the VVPM and the UPM, yielded identical results and the discussion continued with the VVPM only, which showed much better performance than the first group of the models in GLD porometry data analysis. In subsequent work [9], the GLD porometry data have been combined with the experimental liquid permeability and membrane porosity data to estimate pore non-uniformity as well as tortuosity of the membranes. This is advancement in the porometry data analysis, but the obtained results raise some new questions that are related with the resistance to gas flow through capillaries:

i) The PM, KM and FM with constant viscosity concept are found to be case-sensitive (in some cases reproduce the gas flow data satisfactorily and in others not). And even in the cases when the models treat the porometry data well, the pore number distribution could not be adjusted to predict the liquid permeability unless the gas viscosity in porometry is considered to be much different from the values reported in literature. Hence, the gas viscosity appeared not only to be model dependent, but also different for different membranes. Thus, practically, not much information about the membrane-resistance to flow could be gained from the estimated viscosity value.

ii) The VVPM with the assumption of the variable viscosity reproduced the gas flow porometry data perfectly for membranes with communicating or isolated pore structure. It was anticipated that the gas viscosity would vary, but the estimated value was far different from

that reported in literature; again it was difficult to find any correlation between the viscosity and the pore-number distribution. Equating the pore-diameters to that estimated by Young-Laplace equation leads, in some cases, to porosity much higher than unity. The estimated porosity had to be adjusted through assumption of the pore non-uniformity and the tortuosity.

The intrinsic desire of an analyst to predict liquid permeability from GLD porometry data will remain unfulfilled as long as the effective viscosity or overall resistance to flow remains unknown or unpredictable. Thus, in spite of the potential of the VVPM to treat the GLD porometry data of membranes with different pore-structure, it will not predict their liquid permeability. A more appropriate flux equation is yet to be found.

As early as in 1909, Knudsen [10] reported about specific flow behavior of gases through capillaries, in cases when the mean free path of the gas is of the same order as that of the diameter of the capillaries. The proposed flow equation consisted of two components: conventional Poiseuille flow and Knudsen (called so in later years) flow. The Knudsen term contained empirical constants specific for the flowing gases and capillary diameter. In 1954, Weber [11] proposed a more organized mathematical structure to Knudsen flow equation, in which the Knudsen component of the flow depended on the Knudsen number (*Kn*). The gas flow regime in GLD porometry analysis of microfiltration membranes is also of mixed Poiseuille-Knudsen type, and both the Poiseuille flow and the Knudsen flow contribute to the overall flow. Therefore, in VVPM, the viscosity estimated from the dry flow porometry data implicitly carries the weight of the contribution of Knudsen flow and appears to be pressure-dependent. However, the Weber model (WM) describes both Poiseuille flow and Knudsen flow explicitly assuming that the gas viscosity is constant. Thus, the WM in combination with the Young-Laplace equation could also be applied

to treat the GLD porometry data, and the results should be compared with those of the VVPM. This would give the opportunity to evaluate the potential of so far used gas flux models in treating porometry data and finally also to predict liquid permeability through the membrane.

In fact, more than 20 years back, two research groups (Schneider and Uchytil [12] and Calvo et al. [13]) were the first, to the authors' knowledge, to analyze the gas flow data obtained by the GLD method adopting a version of the formulations introduced by Weber [11]. However, they did not achieve significant success in predicting the liquid permeability of investigated membranes. The first group [12] analyzed the data developing a porosity distribution function and derived a flux equation in which the Poiseuille component of flow appears to be a function of pressure difference across the membrane only (the influence of actual pressure on the measured gas flow has thus been masked). The second group [13] ignored the compressibility of the porometry gas in treating the data. Overall, the procedure for GLD porometry data analysis developed by those authors remained without noticeable follow up.

In the present paper, an analysis has been made on the approximations in adapting the WM (that is primarily developed for gas flow through a well-defined capillary) to describe the gas flow through a porous body consisting of communicating and/or non-communicating capillaries with different shapes, sizes and tortuosity. Then, GLD porometry data of three different classes of microfiltration (MF) membranes, which are relevant for research or industrial applications, have been treated:

i) three poly(ethylene terephthalate) (PET) track-etched membranes with different pore size distribution ranges (cf. [8]),

ii) a polyethersulfone (PES) (cf. [8,14]), a polyvinylidene fluoride (PVDF) (cf. [15]) and a polypropylene (PP) membrane (cf. [8]), prepared by different polymer solution film casting cum phase separation methods, and

iii) a polytetrafluoroethylene (PTFE) membrane prepared by polymer extrusion and stretching (cf. [16]).

Thus, the membranes under investigation cover a comparatively wide range of MF membrane types with different pore morphologies. In this paper, a methodology for GLD porometry data treatment based on WM is developed first. The applicability of the WM is then tested with the experimental porometry data. All results for the different membranes are thereafter critically discussed and also systematically compared with those obtained from data analysis using VVPM, with respect to the parameters to describe the flow and the output in terms of pore characteristics of the different membranes.

2. Weber model for gas flow through capillaries under Poiseuille-Knudsen regime

The gas flow rate, Q, (m^3/s) (recalculated at atmospheric pressure P_a) in a capillary with a specific diameter, D, is given by the following relation [11]:

$$Q = \left(S \frac{\bar{u}_m}{P_a} \frac{\pi D^3}{12} + \frac{\pi D^4}{128 \eta_w} . p \right) \left(- \frac{\Delta P}{L} \right) \text{ with } \bar{u}_m = \sqrt{\frac{8RT}{\pi M}} \text{ and } p = \frac{P_{av}}{P_a} \quad (1)$$

where S is a coefficient accounting for the contribution of Knudsen flow and slippage factor, $\bar{u}_m$ is the average molecular velocity of the gas, η_w is the gas viscosity, p is a dimensionless pressure, expressed by the ratio of the mean of the feed and the exit-side pressures, P_{av}, and the atmospheric

pressure, P_a, and $-\Delta P$ is the pressure difference applied between the two sides of the capillary, L is the capillary length, M is the molecular mass of the gas, R is the universal gas constant and T is the absolute temperature.

The viscosity, η_w, in Equation (1) is a constant and might (under certain circumstances) be equal to the viscosity of the gas as available in literature. The coefficient S is not a constant, rather a complex function of Knudsen number, Kn, defined as $Kn = \lambda/D$; where λ is the mean free path of the gas. Since λ depends on pressure, for a given capillary even with uniform cross-section, it varies with pressure. Thus, Kn will vary along the capillary length for a given pressure arrangement, and also with the variation of applied pressure. The value of S is proposed to be estimated by the expression $S = (\nu+Kn)/(1+Kn)$ with $\nu = \pi/4$, $3\pi/16$ or 1 [12]. Dullien [17] described gas flow in a capillary according to Hagen-Poiseuille with an equation identical with the Equation (1), but replacing the coefficient S with a constant value of $3\pi/16$. Instead, Shrestha et al. [18] assumed that S is equal to unity. Scott and Dullien [19] analyzed flow of diluted gases assuming that the slippage factor at the capillary wall also contributes to the overall flow. Its contribution is described by an expression identical with that of Knudsen flow; as such the coefficient S in Equation (1) should account for contribution of both Knudsen and slippage factor. No precise kinetic gas theory-based treatment of the flow exists in the transition region, where λ and D are of the same order.

In GLD porometry analysis, the pore structure of a microfiltration membrane (consisting of communicating or non-communicating pores) is replaced by different classes of isolated capillaries. Thus, the gas flow through a dry membrane is given by the following relation:

$$J_d = \left(\frac{\bar{u}_m}{P_a}\frac{\pi\sum S_i n_i D_i^3}{12} + \frac{\pi\sum n_i D_i^4}{128\eta_w}.p\right)\left(-\frac{\Delta P}{L}\right) \quad (2)$$

where n_i is the pore-number density of the i-th class pores with diameter D_i. The subscript d stands for the dry run porometry data.

As the value of the coefficient S for flow even in a single capillary in Equation (1) could not be evaluated precisely, it is hard to expect that the values of the coefficients S_i, as they appear in Equation (2) for flow through porous bodies could be determined separately and precisely. Instead, it is reasonable to assume that the coefficients S_i will be different for different capillaries, and even for a given capillary, S_i would depend on the pressure arrangement. This introduces uncertainty in the analysis of porometry data with the WM.

Schneider and Uchytil [12] reviewed that for the majority of porous solids (e.g., catalysts, adsorbents, etc.) ν was equated to unity, and as such, in porometry data analysis the value of S would appear constant at unity independent of Kn. Calvo et al. [13], on the other hand, assumed that up to certain pore diameter value, the flow is predominantly Knudsen type, while above that threshold value the flow is Poiseuille type. Thus, they divided porometry data in two parts, for the separate parts they applied either Knudsen or Poiseuille equation. Some other authors [20,21] proposed S to be adjustable. In fact, an adjustable S value averaged over all the capillaries is very convenient to handle the GLD porometry data, and such approach will be adopted in this work.

Rewriting Equation (2) in terms of permeability, ξ, one obtains:

$$\xi_d = S_{av}\frac{\bar{u}_m}{P_a}\frac{\pi\sum n_i D_i^3}{12} + \frac{\pi\sum n_i D_i^4}{128\eta_w}.p \quad (3)$$

with

$$\xi_d = \frac{J_D . L}{(-\Delta P)} \text{ and } S_{av} = \frac{\sum S_i n_i D_i^3}{\sum n_i D_i^3} \quad (4)$$

If S_{av} could be approximated by an adjustable constant value, the ξ_d vs. p plot will be a straight line. Those experienced in the art, however, must admit that the ξ_d vs. p data can only rarely be approximated by a straight line over wide ranges of pore-diameters and applied pressures. This is completely expected, as S_i being a function of Kn, it is different for different classes of pores under identical pressure arrangements. Moreover, pores of a real membrane are of non-uniform cross-sections and tortuosity. Such membranes, when replaced, in porometry data analysis, by an equivalent model membrane with uniform cross-section also carry some weight of non-uniformity and tortuosity. Thus, the Equation (3) could be applied in GLD porometry data analysis only if it represents a straight line within experimental error, and that limits its application to membranes with narrow pore-size distribution only.

2.1 Data Treatment procedure

The GLD data treatment procedure and the derivation of important formulae for that purpose are described below. The gas flow data from the two parts of the GLD permporometry experiment, permeation through the dry and the wet membrane, respectively, will below be referred to as “dry flow porometry” data and “wet flow porometry” data, respectively. The dry and wet flow data acquisition procedure is described in details in Appendix B in SI.

2.1.1 Initial test of the applicability of the WM in GLD porometry data analysis

The GLD dry flow porometry data is fitted to the Equation (3) rewritten in suitable form (i.e., Equation (5)) for further treatment.

$$\xi_d = \frac{J_d}{-(\Delta P/L)} = \left(\alpha_1 \sum n_i D_i^3 + \alpha_2 \sum n_i D_i^4 \,.\, p\right) \tag{5}$$

with

$$\alpha_1 = S_{av} \frac{\pi \bar{u}_m}{12 P_a}, \alpha_2 = \frac{\pi}{128 \eta_w} \tag{6}$$

A satisfactorily linear plot of ξ_d vs. p data throughout the data acquisition range (beginning with the pressure that corresponds to the first measurable flow in wet run and ending at the pressure that corresponds to the point of intersection between the dry and the wet curves) would give the first indication about the preciseness with which the pore-size distribution will be determined. Furthermore, this operation will give the information to what extent this distribution would predict the liquid permeability of the membrane, and whether this is obtained without making any further analysis (how it is realized is described below).

Assigning

$$m_1 = \alpha_1 \sum n_i D_i^3 \text{ and } m_2 = \alpha_2 \sum n_i D_i^4 \tag{7}$$

Equation (5) takes the form:

$$\xi_d = (m_1 + m_2 . p) \tag{8}$$

The liquid flux through the same membrane is described by the following relation:

$$J_l = \frac{K_{D,l}}{\eta_l}\left(-\frac{\Delta P}{L}\right) \text{ with } K_{D,l} = \frac{\pi \sum n_i D_i^4}{128} \tag{9}$$

where the subscript *l* stands for the permeating liquid and $K_{D,l}$ is the Darcy coefficient as observed in liquid permeation experiments.

By combining Equations (6) and (7) and considering the expression for Darcy coefficient in the right hand side of the Equation (9), one obtains:

$$m_2 = \frac{K_{D,g}}{\eta_w} \tag{10}$$

Where $K_{D,g}$ is the equivalent term for Darcy coefficient in gas permeation experiments.

From the slope, m_2, of the linear ξ_d vs. p plot, the value of $K_{D,g}$ can be calculated (with Equation (10)), if η_w is assumed to be equal to the viscosity of the gas used in porometry data acquisition, η_a, as available in reference books (this step will be called "*viscosity adjustment*"). The estimated $K_{D,g}$ value from the GLD porometry data could now be compared with the $K_{D,l}$ value obtained from liquid permeation experiment (cf. Equation (9)). If the two values of the same parameter (Darcy coefficient), K_D, differ beyond acceptable limit, precise analysis of the GLD porometry data shall never give pore-number distribution that would predict the liquid permeability of the investigated membrane. If the final goal is the liquid permeability prediction, the calculation might be interrupted immediately. However, as one of our main tasks is to find the stumbling block that prevents achieving liquid permeability prediction, the calculation will continue for estimating pore-number distribution and membrane porosity (see section 2.1.2).

There is a second option in this analysis. To ensure success in the prediction of liquid permeability, as done in previous analyses [8,9], the $K_{D,g}$ value from the porometry data (cf. Equation (8)) will be equated with the $K_{D,l}$ value obtained from liquid permeation experiment (this step will be called "K_D *adjustment*"). The value of η_w will be adapted from Equation (10). Thus, η_w will appear as a model dependent parameter (of the Weber model in this case). The more η_w approaches η_a, the better the estimated pore-size distribution predicts the liquid permeability. In fact, the adapted

value of η_w will show what the viscosity value should have been equal to, for the GLD porometry data to predict the liquid permeability of the membrane.

Further analysis with the intercept of the linear ξ_d vs. p plot could not be done at this stage. However, the basic criterion for the preciseness of the analysis of the wet flow porometry data has been established from the dry flow porometry data and that is as follows:

$$\sum(n_i D_i^3)_w = \frac{m_1}{\alpha_1} \text{ and } \sum(n_i D_i^4)_w = \frac{m_2.128\eta_w}{\pi} \text{ with } \alpha_1 = S_{av}\frac{\pi\bar{u}_m}{12P_a} \qquad (11)$$

where the index *w* stands for quantities derived from wet flow porometry data analysis (compare Equation (11) with the corresponding Equation (7)). In Equation. (11), the term in the left hand side is calculated based on the pore-size distribution data set (n_i, D_i) estimated from the analysis of the wet flow porometry data, but the term in the right hand side of the equation is obtained from the dry flow porometry data (cf. Equation (7)). For precise determination of pore-number distribution, both conditions, in Equation (11), must be satisfied simultaneously.

2.1.2 Estimation of pore-size distribution data set (n_i, D_i)

The pore-size distribution data set (n_i, D_i) is obtained from the analysis of wet flow porometry data. For this purpose, the (P_{av}, D) data series has to be generated first. The porometer software provides (-ΔP, Q) data series. Each pressure increment step corresponds to the opening of new pores with a definite size of the diameter as described by the Young-Laplace equation (Equation (12)).

$$D = \frac{4\sigma}{-\Delta P} \qquad (12)$$

where σ is the surface tension of the pore-filling liquid.

Knowing that the exit side pressure is equal to the atmospheric one, P_a, the data series (P_{av}, D, ξ_d) can be easily generated from the available ($-\Delta P$, Q) data generated by the porometer software.

Following from Equation (5) for permeability in dry flow, ξ_d, permeability in wet flow, ξ_w, at the (m-1)-th pressure increment step, $\xi_{w,m-1}$, is expressed as follows:

$$\xi_{w,m-1} = \left(\alpha_1 \sum_{i=1}^{m-1} n_i D_i^3 + \alpha_2 \sum_{i=1}^{m-1} n_i D_i^4 \,.\, p_{m-1} \right) \tag{13}$$

Rewriting Equation (13) for the m-th pressure increment step and combining it again with the same, one obtains:

$$n_m = \left[\left(\xi_{w,.m} - \xi_{w,m-1} \right) - \alpha_2 \sum_{i=1}^{m-1} n_i D_i^4 \,(p_m - p_{m-1}) \right] \Big/ (\alpha_1 D_m^3 + \alpha_2 D_m^4 . p_m) \tag{14}$$

The Equation (14) will give the required data set (n_i, D_i).

2.1.3 Sequence of operations for determining (n_i, D_i)

a) Generate the (p, D, ξ_d, ξ_w) data series from the ($-\Delta P$, "wet flow" rate, "dry flow" rate) data provided by the porometer software (optionally, apply Equation (12) for generating the pore diameter data).

b) Draw a ξ_d vs. p plot (cf. Equation (8)); determine m_1 and m_2.

c) There are two options to continue (cf. section 2.1.1):

   i) Make "*viscosity adjustment*", i.e. assume η_w = viscosity of gas at normal conditions (e.g. for air, $\eta_a \approx 1.85 \times 10^{-5}$ Pa.s), and estimate α_2 (cf. Equation (6)) and the Darcy coefficient, $K_{D,g}$ (cf. Equation (10)). This $K_{D,g}$ value may be much different from $K_{D,l}$ and as such may not predict the liquid permeability!

ii) Make "K_D *adjustment*", i.e. determine the Darcy coefficient, $K_{D,l}$, from liquid permeation experiment (cf. Equation (9)), substitute it in the position of $K_{D,g}$ and calculate the adapted value of η_w (cf. Equation (10)). Estimate the value of α_2 with this adapted value of η_w (cf. Equation (6)). Compare η_w with the viscosity of the gas used available in literature. This η_w value might be much different from η_a.

d) Assume $S_{av} = 1$ (as the first approximation) and calculate α_1 (cf. Equation (6)).

e) Estimate the two characteristic quantities $\sum(n_i D_i^3)_d$ and $\sum(n_i D_i^4)_d$ using Equation. (7) (note that they are estimated based on dry flow porometry data).

f) Generate (n_i, D_i) data set (cf. Equation (14)).

g) Estimate the two characteristic quantities $\sum(n_i D_i^3)_w$ and $\sum(n_i D_i^4)_w$ from the (n_i, D_i) data set. Those are now estimated based on wet flow porometry data. Compare the values with those of the same quantities obtained in step (e) from dry flow porometry data. If the values of the corresponding quantities differ by less than 5% (Equations (15) and (16)), the pore-size distribution as determined from the wet flow porometry data might be considered acceptable. Otherwise, a new value of S_{av} is to be assumed and the calculation should be repeated from step (d) through step (g) until the Equations (15) and (16) are satisfied. If the values of Δ_3 and Δ_4 do not satisfy the relations as defined by the Equation (15) and (16) for any value of $S_{av} \geq 0$, the estimated pore-number distribution could not be considered precise, and with such distribution, the experimental wet flow and dry flow porometry curves could hardly be satisfactorily reproduced.

$$\Delta_3 = \left| 1 - \sum(n_i D_i^3)_w / \sum(n_i D_i^3)_d \right| \leq 0.05 \qquad (15)$$

$$\Delta_4 = \left|1 - \sum (n_i D_i^4)_w / \sum (n_i D_i^4)_d\right| \leq 0.05 \quad (16)$$

The deviation (Δ_3, Δ_4) of the characteristic parameters in Equation (15) and (16) to be accepted (proposed to be less than 0.05) is bit arbitrary. The smaller this value is chosen/assigned, the higher would be the preciseness of the estimated pore-size distribution, and consequently, the flow data (dry and wet) will be better reproduced. Higher deviation is tolerated, when the validation of the WM itself through step (b) in this sub-section carries some irregularities, which are not the error in data acquisition, rather characteristic of the non-uniformity and tortuosity of pores exerting non-linear response of resistance at different pressure-arrangements. The dry and wet flow data themselves may impose acceptance of higher deviation, but that will definitely manifest in flow reproduction.

2.1.4 *Data analysis performed in this work*

For the 'K_D adjustment' option, i.e. option (ii) in step c) (cf. section 2.1.3), for which it is assumed that $K_{D,g} = K_{D,l}$, and η_w is an adaptable parameter, the tentative value of S_{av} (which could be used instead of assuming $S_{av} = 1$ as the first approximation, to continue with step d)) can be determined from the pressure-dependent viscosity data, η_v, obtained from the VVPM method of analysis as per following linear relation (for details see Appendix A in Supporting Information, SI):

$$\frac{1}{\eta_v} = \frac{1}{\eta_w} + S_{av} \cdot \frac{32\bar{u}_m}{3} \cdot \frac{1}{D_w} \cdot \frac{1}{P_{av}} \quad \text{with } D_w = \frac{\sum n_i D_i^4}{\sum n_i D_i^3} \quad (17)$$

where D_w is named "Weber diameter".

In this work, all the operations described in section 2.1.3 have been performed with a program written on Microsoft Excel sheet. Although two other research groups [12,13] had initiated GLD

porometry data analysis with the Weber model more than 20 years ago, this is the first, to the authors' knowledge, comprehensive and systematic procedure for determining pore-number distribution applying mixed Knudsen-Poiseuille flow model.

3. Results and discussion of membrane characterization by GLD porometry

The GLD porometry data of various MF membranes with different pore morphology have been treated by the methodology described in section 2.1. Details of the methods used for membrane characterization can be found in SI (Appendix B). An overview on the membranes is presented in Table 1; more details can also be found in SI (Appendix B). Besides the information about the manufacturer, fabrication method, pore morphology determined by scanning electron microscopy (SEM) and membrane thickness, it contains GLD porometry data like mean flow pore pressure (MFPP) and mean flow pore diameter (MFPD) obtained as output by the porometer software. The SEM data for PET, PES and PP membranes were presented as Supporting Information to previous work [8,9]; those of the PVDF and PTFE membranes are presented in Figures B1 & B2 (Appendix B, SI) of this work.

Table 1. Overview on the membranes investigated in this work

Membrane material[1]	Preparation method[2]	Manufacturer	Membrane thickness, µm	Mean flow pore diameter (MFPD)[3], µm	Mean flow pore pressure (MFPP)[3], Bar	Pore morphology as seen in SEM
PET: I, II, III*	track-etched	Oxyphen, Switzerland	I: 8 II: 22 III: 33	I: 0.17 II: 0.40 III: 0.49	I: 3.84 II: 1.60 III:1.30	Straight cylindrical pores. I: Overlapping occasional II and III; Overlapping frequent
PES*	NIPS	3M / Membrana, Wuppertal, Germany	108	0.23	2.75	Intercommunicated pores forming network structure
PP*	TIPS	3M / Membrana, Wuppertal, Germany	202	0.29	2.21	Bundles of loosely packed thick fibers yielding porous network
PVDF	VIPS	Prepared in laboratory [15]	98	0.26	2.50	Sponge-like network forming intercommunicated pores
PTFE supported by a PP net	Extrusion and stretching	Pall Corporation	121	0.34	1.91	Network structure in which fine fibrils are interconnected to form nodes. The PP grid at the bottom of the membrane acts as mechanical support

* already analyzed by VVPM in previous works [8,9]

[1] PET: poly(ethylene terephthalate); PES: polyethersulfone; PP: polypropylene; PVDF: poly(vinylidene difluoride); PTEF: polytetrafluoroethylene

[2] NIPS: liquid non-solvent induced phase separation; VIPS: non-solvent vapor induced phase separation; TIPS: thermally induced phase separation

[3] determined by automatic capillary flow porometer CFP-34RTG8A-X-6-LA, from PMI Inc. (United States)

In this work, the GLD porometry data of all membranes shown in Table 1 were treated with the WM by the two options as described in section 2.1.3, step c). In Equation (3) and consequentially in Equation (10), η_w was substituted by air viscosity, η_a, and the corresponding value of $K_{D,g}$ was estimated (option i)). Immediately, it was clear that this $K_{D,g}$ value was much different from the Darcy coefficient, $K_{D,l}$, determined by liquid permeability experiment. But still the calculation was continued for the determination of pore-number distribution. As this option fails to predict liquid permeability, the second option was to equate the Darcy coefficient, $K_{D,g}$, describing gas permeability to the Darcy coefficients $K_{D,l}$ obtained from liquid permeability data, thus making the viscosity parameter η_w adaptable (option ii)); and the calculation was continued as described in section 2.1.3.

The results of VVPM treatment of GLD porometry data of the PET, PES and PP membranes were reported in previous works [8,9]; now this treatment has been extended to the PVDF and PTFE membranes for completeness of the analysis and to enable a comparative evaluation for the two different models, WM and VVPM.

3.1 Validation of the WM with porometry flow data

The model validation is performed at two stages: i) Test for linearity relation between permeability and average pressure, and ii) reproduction of dry flow and wet flow porometry curves with the computed pore-number distribution data. The predictability of the liquid permeability of the membrane may still not be achieved, but the estimated pore-number distribution data must, at least, reproduce the dry flow and wet flow porometry data from which they have been computed. This

test of consistency is neither recommended by the present standards [6,7], nor is it done by any porometer software available in the market.

3.1.1 Test of linear relation between the permeability and the average pressure

Linearity of permeability vs. average pressure plot is the first indication of the applicability of WM in estimating pore-number distribution precisely. This test has been applied for all the membranes under investigation. However, for economy of space, only few representative plots will be shown in the main text, the other plots can be found in SI (Appendix C).

Among the three PET track-etched membranes, PET_I, PET_II and PET_III (in Figs. C1, C2 and C3 in SI, respectively), only the PET_II membrane shows satisfactory fit to the experimental data. PET_I shows very poor fit as the experimental curve shows two distinct slopes in the low and high pressure sections separated by another with sharp increase in slope. PET_III shows extended linear section, but the permeability data in the low pressure range (1.6-2.0 Bar) is seen to be almost independent of pressure. The Knudsen number under this condition lies in the range of 0.07- 0.41 (calculated based on the pore-size-ranges). As seen in Equation (1), S as a measure for contribution of Knudsen flow through a well-defined capillary is not a constant, but depends on pressure. For a given average pressure, S depends on D as well. The dependency of S on pressure is more exposed in the low pressure-ranges. In treating the dry flow porometry data, a constant average value of S is assumed independent of the pressure and the pore-sizes. In addition, the pores are also not uniform. Thus, assumption of constant average S might be one of the major reasons for deviation of the permeability curve from linearity in the low pressure-ranges.

The permeability vs. pressure plots for PES, PP, PVDF and PTFE membranes are shown in Fig. 1. To accommodate the curves in a single figure, permeability data have been multiplied by a scale

factor, γ. For better view of the curve-fitting, the individual plots for the four membranes are given separately in SI (Figs. C4 to C7). As seen in Fig. 1, among the four membranes, the plot of the PTFE membrane shows perfect linear fit. For the other three membranes, although the relations have been approximated by a straight line, significant deviations can be noticed.

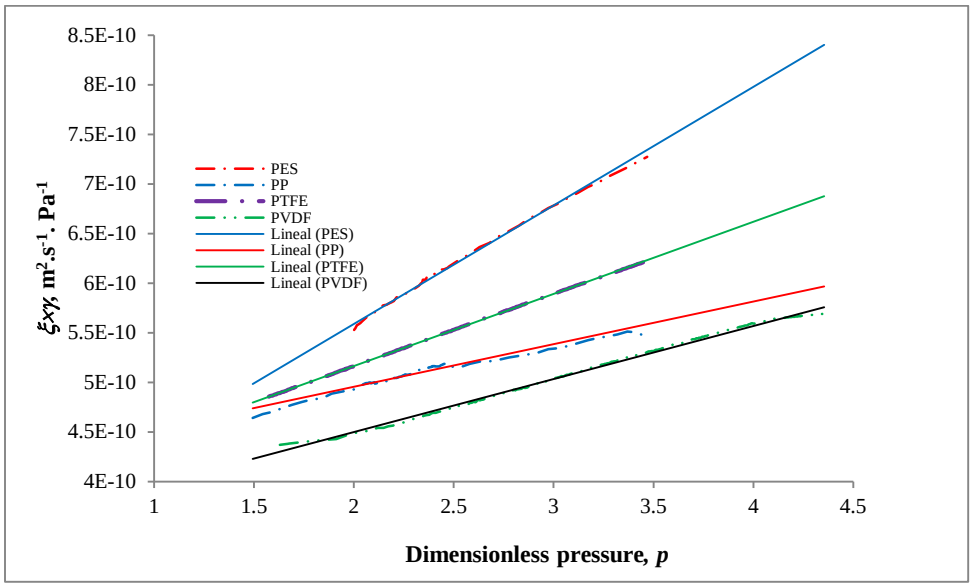

Figure 1 Permeability, ξ, (multiplied by scale factor, γ) vs. dimensionless pressure, p, plot for PES ($\gamma = 2.00$), PP ($\gamma = 1.30$), PTFE ($\gamma = 0.50$) and PVDF ($\gamma = 1.25$) membranes.

3.1.1.1 Determination of pore-number (both relative and absolute) distribution

The pore-number distributions (both relative and absolute) of the membranes have been determined for both options, i.e. viscosity adjusted and K_D adjusted (as described in step c in section 2.1.3). In applying the WM for analysis, the maximum deviation of the two characteristic parameters, Δ_3 and Δ_4, (cf. Equations (15) and (16)), were found to be below 0.02 (with the

maximum deviation for precise analysis proposed to be 0.05) for all membranes except for the PVDF membrane, for which the deviations, Δ_3 and Δ_4, were as high as 0.09 for both options.

Hence, it is found that both options of WM could be applied to determine the pore-number distribution, and that these distributions reproduce the porometry flow data equally well. For comparison, the pore-number distribution has also been determined by the methodology based on VVPM [8,9] and the reproduction of the porometry flow data have been compared with those done by the WM (discussed below in sections 3.1.2 & 3.1.3).

3.1.2 *Obtained pore number distribution*

The relative and the absolute pore-number distributions of the membranes have been determined by both options in WM. Definitely, the absolute pore-number distributions (APND) is more informative and can be used to estimate the Darcy coefficient for permeability and also the porosity of the membrane. For economy of space, the relative and the absolute pore-number distributions, respectively, of all membranes under investigation are presented in SI (Appendix D, Figs. D1-7, and Appendix E and F, Figs. E1-7 and F1, respectively). The relative pore-number distribution for each of the membranes is found to be identical (completely overlapping) for both options in WM (Figs. D1-7, SI). The APND is similar for the two options of data analyses, except that the absolute numbers of pores for a given diameter vary for the two options (Figs. E1-7). This is reasonable as the Poiseuille component, m_2 (Equation (5)), determined in validation of WM remains the same for the two options, and for each of them either the numerator is adjusted and the denominator is estimated or vice-versa. The behavior of the relative and the absolute pore-number distribution are described in detail in Appendix F (SI) Different from the other cases with more or less monomodal

pore size distributions, the PVDF membrane shows a multimodal distribution with pores in very different diameter regions (Figs. E7a,b).

For a more detailed discussion, data of two representative membranes are presented in Figs. 2 and 3. The first shows the absolute pore-number distribution of the PTFE membrane, a representative of the membranes satisfying very well the condition for maximum acceptable deviation of the two characteristic parameters, Δ_3 and Δ_4 (all the membranes, except PVDF, fall in this category). The pore-number distribution data of the PVDF membranes, a representative of those failing to satisfy the tolerance limit for Δ_3 and Δ_4 for precise analysis, are presented in Figure 3.

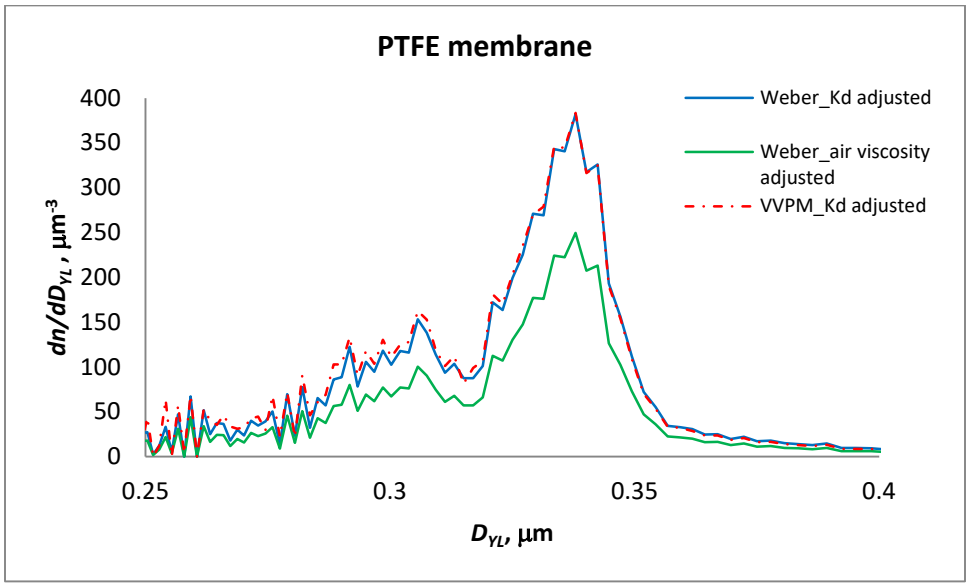

Figure 2. Differential pore-number (absolute) density distribution of PTFE membrane determined by Weber model (two options) and VVPM

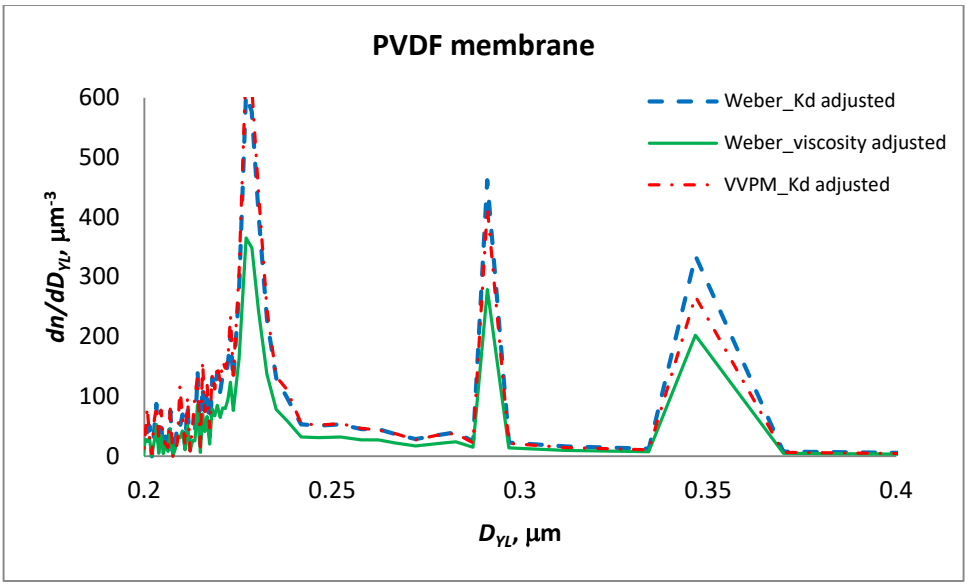

a)

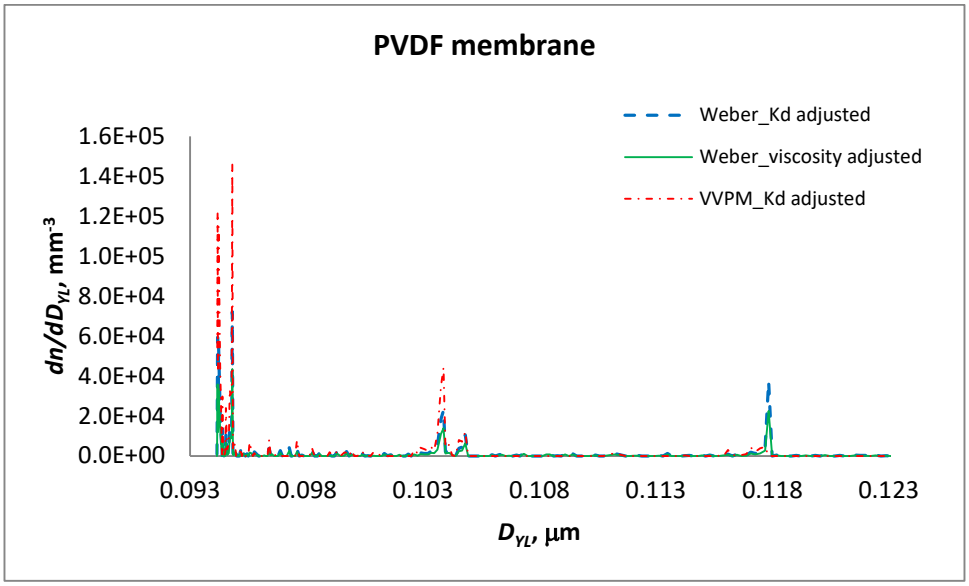

b)

Figure 3. Differential pore-number (absolute) density distribution of PVDF membrane determined by Weber model (two options) and VVPM: **a)** partial view in the range of 0.2 to 0.4 µm; **b)** partial view in the range of 0.09 to 0.123 µm.

As seen in both the Figures 2 and 3, the absolute pore-number distributions of PTFE and PVDF membranes estimated by the two options of the WM and by the VVPM are similar, differing only

in the magnitude relative to the pore-number axis. Among the two options of the WM, the one with viscosity adjustment estimates the number of pores for a given diameter much lower than the second option with K_D adjustment. This pattern of lower absolute pore-number density for the first option was found for the PET, PES and PP membranes as well (see Figs. E1-5 in SI). For better visibility, the absolute pore-number distributions of PTFE and PVDF membranes estimated by the two options of the WM only (excluding that by VVPM) have been presented in see Figs. E6, E7a & E7b in SI).

For the PVDF membrane, the pore-number distribution is highly uncommon. The large-sized pores are found in three distinct sections in the range of 0.2 to 0.4 μm (Fig. 3(a)). There are also pores in a very narrow range of pore diameters, 0.093 to 0.12 μm, which are 2 to 4 times smaller than the large pores (Fig. 3(b)). Generally, it is assumed that small-sized pores would have very small contribution to flux. The ordinate values for the VVPM-derived and WM-derived (with K_D adjustment) curve around pore diameter of 0.093 μm (Fig. 3.3b), however, are about 30 fold higher than those for the larger pores (Fig. 3(a)); in a common plot (shown separately as Figs. G1 & G2 in Appendix G, SI), the peaks in the range of 0.2-0.4 μm are almost invisible. Thus, as per both VVPM and WM, the pores around 0.093 μm are also expected to contribute to flow in an appreciable amount.

3.1.3 *Test of reproducibility of wet and dry flow data*

With the estimated (n_i, D_i) data series from WM with both options as described in section 2.1.3, the dry flux and wet flux data for the membranes have been calculated by Equations (3) and (13) (i.e., multiplying the permeability by pressure gradient), respectively. The calculated and the

experimental flux curves of the PET, PES and PP membranes are presented in SI (Appendix H, Figures H1-5); those of PTFE and PVDF membranes can be seen in Figs. 4 and 5.

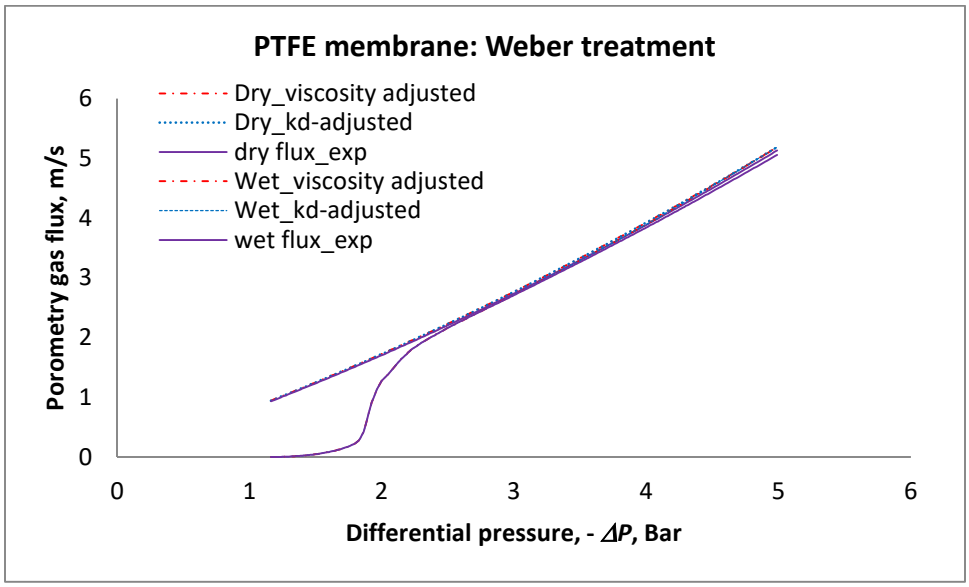

Figure4. Porometry flux reproduction for PTFE membrane with WM, options 1 & 2

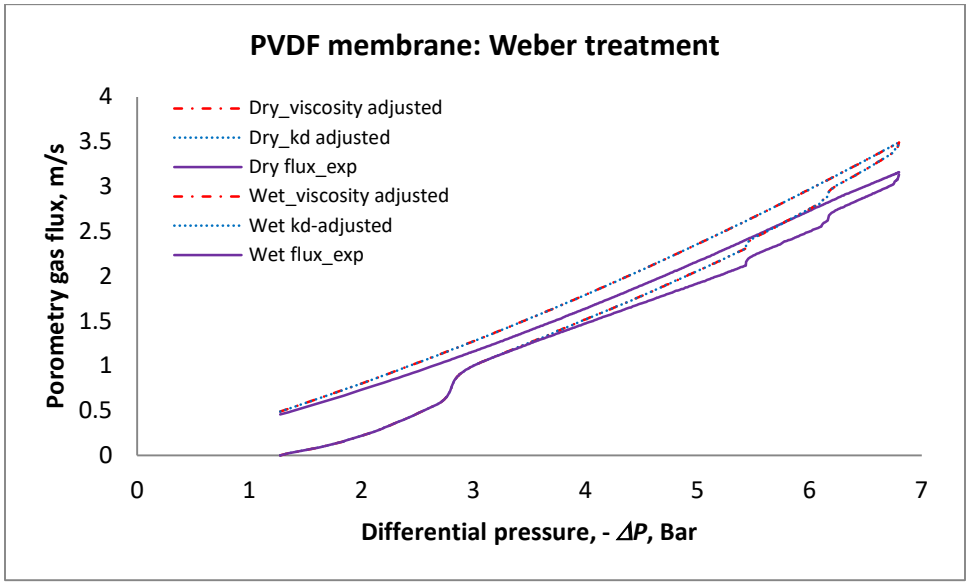

Figure 5. Porometry flux reproduction for PVDF membrane with WM, options 1 & 2

The results for the WM (with both the options 1 & 2), the main focus of this study, can be summarized as follows: i) for PET_I, the wet flux is reproduced perfectly, but the dry flux only with some deviation (Fig. H1 in SI), ii) for PET_II (Fig. H2 in SI), PES (Fig. H4 in SI), PP (Fig. H5 in SI) and PTFE (Fig. 4), both the wet and dry fluxes are reproduced almost perfectly, iii) for PET_III, both the wet and dry fluxes are reproduced with some deviations (Fig. H3 in SI), and iv) for PVDF (Fig. 5), both the wet and the dry fluxes are reproduced only with larger deviations. Overall, for the PET, PES, PP and PTFE membranes, the variation between the calculated and experimental fluxes does not exceed 5%. For PVDF membrane, however, the variations reach around 9%.

The porometry flux reproduction test for VVPM for PET, PES and PP membranes was reported in previous works [8,9]. In this work, results of this test for PTFE membrane are shown in SI (Figure I1, Appendix I) and for PVDF membrane in Fig. 6. As for PET, PES and PP membranes [8,9], also for PTFE and PVDF membranes, the VVPM reproduces the porometry fluxes almost perfectly.

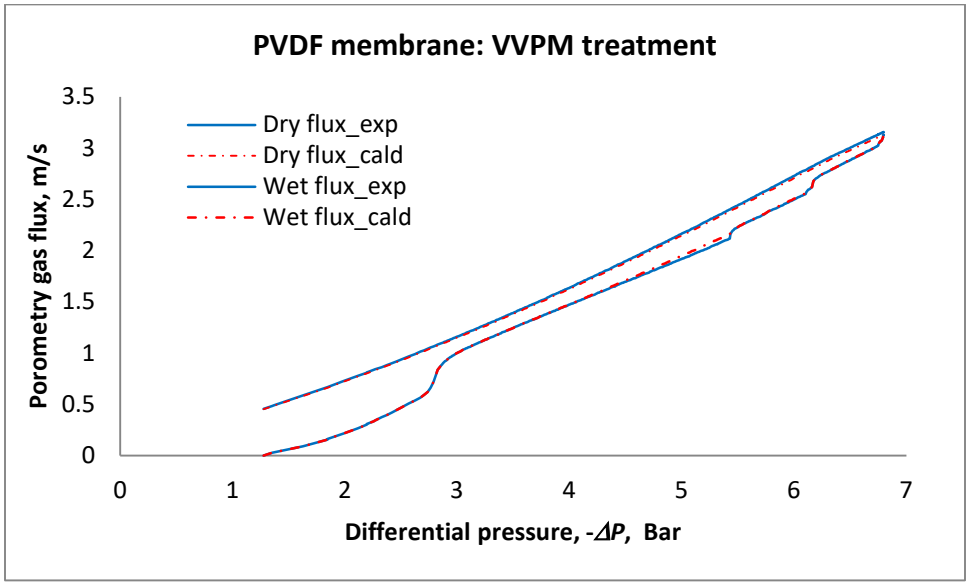

Figure 6. VVPM validation with dry and wet flow porometry data of PVDF membrane

The wet flow curve for the PVDF membrane reveals several steps (cf. Fig. 6). As seen in Fig. 3 (also separate illustrations in Figs. E7a,b and G1 & G2, SI), both the VVPM and WM estimated a very high fraction of pores with diameter around 0.1 μm and their contribution to flow seems significant. The flow behavior through PVDF membrane is highly specific and still the pore size distribution as determined by VVPM reproduces both the dry and wet porometry flux almost perfectly. The WM also detect the multimodal pore-size distribution with high concentration of pores in the range of 0.09 to 0.123 μm, but does not reproduce the wet and dry porometry flow so satisfactorily, but still the variation between the experimental and calculated flow is less than 10%, which is within the flux variation from specimen to specimen of a membrane sheet. Although for the other membranes, the reproduction of wet and dry fluxes by VVPM and WM did not vary appreciably, and the specific pore-distribution of the PVDF membrane is also detected by both the models, still the VVPM and WM reproduced flow pattern differently. From the data of a single membrane, any overall conclusion could not be drawn about the superiority of any model, rather it may be speculated that since VVPM estimates the apparent viscosity values from the experimental dry flux at every pressure-increment, the error in data treatment is minimized. For WM, however, assumption of a constant average value for the coefficient *S* in Equations (2) and (3) for flow through membrane with multimodal pore-distribution results in bit 'high' approximation and that could bring some additional error in the flux prediction.

Overall, validated by the results of the two tests ((i) linearity of permeability vs. average pressure and (ii) reproducibility of wet and dry flux from the estimated pore-distribution) within the range

of different membranes, it can be concluded that the Weber model (WM) could also, alternatively to the VVPM model, be applied to determine the pore-size distribution from GLD porometry data.

4. Model-dependent GLD porometry data treatment: Implications with respect to the analysis methods and the output about porous membrane structure

The results of section 3 indicate that GLD porometry data can be treated by the recently proposed VVPM [8,9] as well as by the WM. The VVPM is basically the well-established Hagen-Poiseuille model for gas flow through porous bodies consisting of cylindrical capillaries without any slippage at the capillary wall, but with an adapted viscosity value to fit the observed flow data to the model. The WM considers both Knudsen and Poiseuille flows through capillaries. Thus, from the viewpoint of flow mechanism, the WM is more appropriate for describing gas flow through capillaries for which the mean free path of the molecules is in the same order with the capillary diameter. However, as found in previous works [8,9] as well as in this work, the method of data treatment by the VVPM is much simpler and – at least in some cases – more precise than that by the WM. Thus, in this respect, the VVPM will be preferable for such analysis of GLD porometry data. What is, however, not achieved with these models is the prediction of liquid permeability from the porometry data analysis. Instead, the porometry data has been supplemented by experimentally obtained liquid permeability data to determine the absolute pore-number distributions. Still the WM has given some additional information which is not available from the VVPM, and that information might indicate the basic reason behind the failure in predicting liquid permeability from GLD porometry data.

Table 2 summarizes some important parameters of the membranes that have been extracted from the porometry data analyzed by the WM, option 1 ("viscosity adjusted"). In fact, this option is the "conventional" analysis by the WM, as it applies the viscosity value of the porometry gas as available in literature, while in WM, option 2 ("Darcy coefficient adjusted"), the viscosity value of the porometry gas is an adapted value and is different for different membranes. Therefore, option 1 is a good basis for analyzing the discrepancy between the experimental and calculated values for the liquid permeability through the membranes and the membrane porosity.

For a given capillary, the Knudsen number *Kn*, characterizing the flow regime, varies as the applied pressure varies; and also for a given applied pressure, the flow regime varies along the capillary length. The capillaries representing membrane pores are of different diameters, and therefore the *Kn* value in GLD porometry data acquisition can vary in a range. Thus, the *Kn* value estimated for flow in a capillary with diameter equal to the "Mean Flow Pore Diameter (MFPD)" at "Mean Flow Pore Pressure (MFPP)", Kn_m, is an averaged value (column 4, Table 2). The actual *Kn* values are different for different capillaries, but are of the same order as that of Kn_m. Similarly, $(J_p/J)_m$ is also an averaged value of Poiseuille contribution to "dry flow" (column 5, Table 2), calculated as $(J_p/J)_m = m_2*p_m/(m_1+m_2*p_m)$, where the index *m* represents MFPP (cf. Equation (8); the Poiseuille contribution at other pressures can also be estimated from the same equation). Both Kn_m and $(J_p/J)_m$ values show that the gas flow regime during the GLD porometry data acquisition is mixed Knudsen-Poiseuille type. Thus, the WM model may be considered to be a proper choice for treating porometry flux data. Contrary to the assumption by other authors [12], that for most porous bodies *S* equals to unity, the averaged value of *S* for some membranes, S_{av} (column 6, Table 2), however, is found to be much higher and even reaches 3.4 (for PP membrane).

Table 2 Parameters describing flow regime during GLD porometry analysis and macroscopic permeability and pore characteristics for all membranes as estimated by Weber model, option 1 ("viscosity adjustment", $\eta_w = \eta_a = 1.85\times10^{-5}$ Pa.s) [+]

Membrane	$K_{D,exp}$ $\times10^{16}$, m^2	ϵ_{exp}	Kn_m	$(J_p/J)_m$	S_{av}	$n_T\times10^{-12}$, m^{-2}	$K_{D,cald}$ $\times10^{16}$, m^2	ϵ_{cald}	D_w, µm
PET_I	0.716	0.08	0.135	0.38	0.89	3.37	0.625	0.072	0.167
PET_II	5.87	0.24	0.091	0.28	1.94	0.557	2.427	0.053	0.388
PET_III	5.82	0.24	0.081	0.26	1.49	0.457	4.276	0.063	0.477
PES	84.5	0.64	0.119	0.47	0.69	14.8	9.823	0.588	0.233
PP	69.9	0.65	0.114	0.17	3.41	3.97	6.097	0.206	0.325
PTFE	40.9	0.78	0.100	0.26	1.90	11.0	26.88	0.804	0.331
PVDF	13.0	0.78	0.108	0.28	1.79	27.6	8.617	0.523	0.251

[+] Kn_m: average Knudsen number estimated for flow at MFPP in a capillary with diameter equal to MFPD; $(J_P/J)_m$: contribution of Poiseuille flow to total flow through the dry membrane at MFPP; n_T: total pore-number density; ϵ: porosity ($=\sum n_i\pi D_i^2/4$); D_w: Weber pore diameter; subscript "exp": experimental value; subscript "cald": calculated value; definitions: MFPP is the pressure at which the wet flow curve (J_w *vs.* $-\Delta P$) intersects the half of dry flow curve ($0.5J_D$ *vs.* $-\Delta P$) and MFPD is the diameter that the MFPP corresponds to as per Young-Laplace equation.

The WM, option 1, has two important credentials as a method for determining MF pore size distribution from GLD porometry flow data: i) The pore-number distribution estimates an averaged diameter (defined as Weber diameter, D_w; cf. section 2.1.4); as can be seen in Table 2

(column 6) that is for all membranes very near to the MFPD (cf. Table 1), and that encourages trust in the method, and ii) it reproduces satisfactorily both the dry flux and wet flux porometry data for all membranes (cf. section 3.1.3). Among the shortcomings are the gross mismatch between the experimental and the calculated values of the Darcy coefficient for liquid permeability (compare columns 2 and 8, Table 2) and the porosity (compare columns 3 and 9, Table 2) of the membranes. Matching with porosity and liquid permeability is not a requirement to authenticate the estimated pore-size distribution as per any standard method [6,7]. Even the reproduction of the porometry flux data from which the pore-size distribution data itself has been extracted (cf. section 3.1.3) is not required to be recognized as a reliable method. Thus, with the capability of reproducing the dry and wet flow data, the developed methodology with WM for $\eta_w = \eta_a$, can be considered a reliable method.

The mismatch between the experimental and the calculated porosity value might be eliminated with the introduction of descriptors for non-uniformity, tortuosity or ineffective expansion of the capillaries [9]. However, to ignore that the calculated Darcy coefficient is, in some cases, several fold lower than the experimentally obtained value, is not much acceptable. As seen in Equations (3), (8) and (10), by applying the WM the slope of the ξ_d vs. p plot is fixed, and by assigning $\eta_w = \eta_a$, the calculated Darcy coefficient is automatically fixed and cannot be adjusted to the experimentally obtained value.

With view on the requirement “agreement with liquid permeability”, the GLD porometry data has also been treated with WM, option 2 (“Darcy coefficient adjustment”; i.e. $K_{D,g}$ is equated to $K_{D,l}$ obtained from liquid permeability experiment). Beyond the results already shown and discussed

in section 3.1.2, important parameters estimated by the K_D-adjusted WM, and by the VVPM for comparison, are summarized in Table 3.

The Weber pore diameter, D_w, is almost the same as that obtained via option 1 (compare D_w values in Tables 2 and 3). The absolute pore-number distributions obtained from option 1 and 2 are similar but differ in magnitude (cf. Figs. E1-E7 in SI); consequentially the calculated porosity values are different (compare ε_{cald} values in Tables 2 and 3).

In the VVPM for GLD porometry data treatment, $K_{D,g}$ was also equated to $K_{D,l}$ [8,9]. Comparing the adapted values of S_{av} and η_w for the WM and those of the analogous, $S_{av,p}$ and $\eta_{w,p}$, predicted by VVPM for WM (cf. Equation (17); see Appendix J, Figs. J1 & J2 in SI), it is obvious that the WM with adjusted K_D and VVPM are highly interrelated (cf. Tables 2 and 3). The only difference is that in WM, the ξ_d vs. p relation (Equation (3)) is approximated by a straight line assuming S_{av} as a pressure-independent parameter, while in VVPM such validation is not required. Fully satisfactory straight line relation for WM could not always be expected for flow even through a single capillary, not to speak of a porous body. In contrast, the VVPM is free of such approximations and adjusts the viscosity of the gas to fit the flow data to the Poiseuille model at all pressures separately. As a consequence, even for somewhat uncommon types of porometry data, the VVPM model describes the flow data almost perfectly (cf. Fig. 6). Not unexpectedly, the WM shows some deviation of the calculated fluxes from the corresponding experimental ones for such less common membrane type (cf. Fig. 5).

Table 3. Important flow and pore characteristics of the gas/membrane systems as determined/predicted by the K_D-adjusted WM and the VVPM [8,9].

Membrane	ϵ_{exp}	WM					VVPM					
		S_{av}	$n_T \times 10^{-12}$, m^{-2}	$\eta_w \times 10^5$, Pa.s	ϵ_{cald}	D_w, μm	$^{**}S_{av,p}$	$^{**}\eta_{w,p} \times 10^5$, Pa.s	$n_T \times 10^{-12}$, m^{-2}	$^{*}\eta_v \times 10^5$, Pa.s	ϵ_{cald}	D_w, μm
PET_I	0.08	0.75	3.946	2.123	0.085	0.167	(0.76)	(2.18)	3.757	0.822	0.082	0.167
PET_II	0.24	0.80	1.347	4.483	0.127	0.388	(0.80)	(4.513)	1.640	1.27	0.130	0.386
PET_III	0.24	1.09	0.632	2.54	0.086	0.477	(1.06)	(2.538)	0.893	0.849	0.093	0.458
PES	0.64	0.08	128.03	15.91	5.06	0.233	(0.08)	(15.56)	135.58	7.40	5.17	0.230
PP	0.65	0.30	45.24	21.17	2.34	0.325	(0.26)	(16.67)	60.954	3.81	2.81	0.296
PTFE	0.78	1.24	16.751	2.817	1.23	0.331	(1.22)	(2.838)	14.695	0.784	1.20	0.332
PVDF	0.78	1.08	45.699	3.053	0.865	0.251	(1.01)	(3.05)	56.953	0.804	0.898	0.237

$^{*}\eta_v$: gas viscosity at MFPP; **Values (in parenthesis) are obtained from the treatment of VVPM-derived data (Equation (17)), a prediction for corresponding values for WM. The determination of the prediction values is illustrated in Figs. J1 & J2 in SI for PTFE and PVDF membranes

As seen earlier in Table 2, the calculated porosity (by "viscosity-adjusted" WM, option 1) might be different from the experimental one, but the values were less than unity for all the membranes. In Table 3, however, for some membranes, the porosity has been calculated (by "K_D-adjusted" WM, option 2, as well as by VVPM) to be much higher than unity. Such outcome is not so unexpected, as the capillaries have non-uniformity and tortuosity, which have not been considered in this analysis. The calculated porosity can be equalized to the experimental value taking these factors into account. For example, taking the non-uniformity, $\omega = 2.6$,and the tortuosity, $\tau = 1.28$, the calculated porosity of the PES membrane will be equal to the experimental value, 0.64 (instead of 5.06 as appears in the Table 3). Such issues have been dealt with in detail in a previous study [9], and in this work, the non-uniformity coefficient and the tortuosity of the membranes will not be estimated to adjust the membrane porosity as this is not in the focus of the present analysis. Recently, Mourhatch et al. [22, 23] have developed a new methodology based on invasion percolation model [24] to treat GLD porometry data in which the porous structure of a membrane is represented by a three-dimensional (3D) network of interconnected pores, and find that the flow distribution curve shifts to right showing an average pore-diameter higher than that determined by computer software. Such result is in unison with the non-uniformity concept introduced in previous work [9] to adjust membrane porosity, in which effective diameter of the membranes with interconnected porous appears higher than that estimated with the assumption of uniform cylindrical capillaries.

The Weber diameter, D_w, has been estimated to be almost the same for the VVPM and the WM (in both options). Thus, assigning $K_{D,g} = K_{D,l}$, both the WM and the VVPM leads to a pore-number distribution that describes the gas flow as well liquid flow through the membranes (Table 3), while assigning $\eta_w = \eta_a$ the WM fails to describe liquid permeability. The main concern that remains

regarding acceptability of the WM (option 2) and the VVPM is that the estimated effective viscosity of the gas is too high to seem to be reasonable. In the VVPM, the viscosity is pressure-dependent, and the value of the gas (air) viscosity shown in column 9 of Table 3 has been estimated at MFPP (because the gas viscosity in the pressure range of porometry data acquisition will be around this value). This viscosity value appears to be as high as 7.4×10^{-5} Pa.s (against 1.85×10^{-5} Pa.s for air at normal conditions as known from literature) for analysis of the PES membrane as one example. Unlike the VVPM, the viscosity in the WM is assumed to be constant, but to equalize the calculated and experimental Darcy constant, the viscosity value that has to be accepted is too high, reaching even 15.91×10^{-5} and 21.17×10^{-5} Pa.s for analysis of the PES and the PP membrane, respectively, as extreme examples. Overall, the model-adjusted viscosity value of the porometry gas varies from model to model and from membrane to membrane, and it is difficult to correlate that parameter with some other parameter that could be extracted from the GLD porometry data (e.g. Knudsen number, MFPD, or contribution of Poiseuille flow to the total flow, all optionally also at some moment during porometry data acquisition). Definitely, the viscosity parameter as it appears in the WM or VVPM is not the Newtonian viscosity, rather a measure for effective resistance depending on the gas flow regime and pattern as well as the complex real pore morphology.

Therefore, as long as the effective resistance to gas flow is not correlated theoretically or empirically with the Newtonian viscosity and on that basis ‘some’ parameter (equivalent to pressure-dependent viscosity parameter) obtained for the treatment of the dry flow porometry data, the treatment of wet flow porometry data will not give pore-size distribution that predicts the liquid permeability. Until then, it is recommended to supplement the GLD porometry data with the Darcy coefficient of the membrane obtained from liquid permeation experiment, and both the WM and

the VVPM could be applied to determine pore-size distribution. As already mentioned above, the data treatment with the VVPM is much simpler [8,9], and it generates the gas and the liquid flow data more precisely. On the other hand the WM can give, besides pore-number distribution, a more detailed picture about variations in the flow regime (Poiseuille vs. Knudsen) during the porometry data acquisition (cf. Table 2) and a pressure-independent viscosity, which gives an idea about the degree of resistance the membrane exerts to the flow (cf. Table 3). As long as the resistance to flow is not precisely described by some empirical relation, it is difficult to assess which of the two models will yield the pore-number distribution that is closer to that of the real membrane.

5. Conclusions

It is concluded that the GLD porometry data can be treated with the Weber model to obtain reliable pore-number distributions of microfiltration membranes. Besides pore-size distribution, the model gives information about the effective resistance to flow through the porous membrane, which is assumed to be a combined effect of gas viscosity, flow regime and pattern, pore morphology and interconnectivity of the pores. It is found that as long as this effective resistance could not be evaluated from the GLD porometry data, liquid permeability through the membrane cannot be predicted. It is recommended that any standard test method for pore-structure characterization must have additional requirements that the estimated pore-number distribution must also reliably predict or describe the liquid permeability of the membrane.

Acknowledgements. The authors express their deep gratitude to the Alexander von Humboldt Foundation for providing financial support to Prof. Dr. Md. Akhtarul Islam for his research stays in 2014 and 2019 at University Duisburg-Essen (UDE).

References

[1] F. Erbe, Die Bestimmung der Porenverteilung nach ihrer Groesse in Filtern und Ultrafiltern, Kolloid Z., 63 (1933) 277-285.

[2] K. Venkataraman, W. T. Choate, E. R. Torre, R. D. Husung, Characterization studies of ceramic membrane. A novel technique using a Coulter porometer, J. Membr. Sci. 39 (1988) 259-271.

[3] G. Reichelt, Bubble point measurements on large areas of microporous membranes, J. Membr. Sci. 60 (1991) 253-259.

[4] L. Zeman, Are pore size distributions in microfiltration membranes measurable by two-phase flow porosimetry?, J. Membr. Sci. 120 (1996) 169-185.

[5] E. Jakobs, W. J. Koros, Ceramic membrane characterization via the bubble point technique, J. Membr. Sci. 124 (1997) 149-159.

[6] ASTM F316, Standard test method for pore size characteristics of membrane filters by bubble point and mean flow pore test.

[7] ASTM E1294, Standard test methods for pore size characteristics of membrane filters using automated liquid porosimeter.

[8] M. A. Islam, M. S. Hossain, M. Ulbricht, Model-dependent analysis of gas flow/pore dewetting data for microfiltration membranes, J. Membr. Sci. 533 (2017) 351-363.

[9] M. A. Islam, M. Ulbricht, Microfiltration membrane characterization by gas-liquid displacement porometry: Matching experimental pore number distribution with liquid permeability and bulk porosity, J. Membr. Sci. 569 (2019) 104-116.

[10] M. Knudsen, Die Gesetze der Molekularströmung und der inneren Reibungsströmung der Gase durch Röhren, Ann. Phys. 28 (1909) 75-130.

[11] S. Weber, Über den Zusammenhang zwischen der laminaren Strömung der reinen Gase durch Rohre und dem Selbstdiffusionskoeffizienten, Dan. Mat. Fys. Medd. 28 (1954) 1-137.

[12] P. Schneider, P. Uchytil, Liquid expulsion permporometry for characterization of porous membranes, J. Membr. Sci. 95 (1994) 29-38.

[13] J. I. Calvo, A. Hernández, P. Prádanos, L. Martínez, W. R. Bowen, Pore size distribution in microporous membranes: II. Bulk characterization of track-etched filter by air porometry and mercury porosimetry, J. Coll. Interf. Sci. 176 (1995) 467-478

[14] M. Ulbricht, O. Schuster, W. Ansorge, M. Ruetering, P. Steiger, Influence of strongly anisotropic cross-section morphology of a novel polyethersulfone microfiltration membranes onto filtration performance, Separ. Purif. Techn. 57 (2007) 63-73.

[15] C. Alexowsky, M. Bojarska, M. Ulbricht, Porous poly(vinylidene fluoride) membranes with tailored properties by fast and scalable non-solvent vapor induced phase separation, J. Membr. Sci. 577 (2019) 69-78.

[16] J. A. Sanmartino, M. Khayet, M. C. García-Payo, H. El Bakouri, A. Riaza, Desalination and concentration of saline aqueous solutions up to supersaturation by air gap membrane distillation and crystallization fouling, Desalination 393 (2016) 39-51.

[17] F. A. L. Dullien, Porous Media: Fluid Transport and Pore Structure, Academic Press, 1979, p. 201.

[18] A. Shrestha, J. Pellegrino, S. M. Husson, S. R. Wickramasinghe, A modified porometry approach towards characterization of MF membranes, J. Membr. Sci., 421-422 (2012) 145-153.

[19] D. S. Scott, F. A. Dullien, The flow of rarefied gases, AIChEJ, 8 (1962) 203-207.

[20] E. Creutz, The permeability minimum and the viscosity of gases at low pressure, Nucl. Sci. Eng., 53 (1974) 107-120.

[21] R. W. Schofield, A. G. Fane, C. J. D. Fell, Gas and vapor transport through microporous membranes. 1. Knudsen-Poiseuille transition, J. Membr. Sci., 53 (1990) 159-171.

[22] R. Mourhatch,T. T. Tsotsis, M. Sahimi M, Network model for the evolution of the pore structure of silicon-carbide membranes during their fabrication, J.Membr. Sci, 356 (2010) 138-146.

[23] R. Mourhatch, T. T. Tsotsis, M. Sahimi, Determination of the true pore size distribution by flow permporometry experiments: An invasion percolation model, J. Membr. Sci.367 (2011) 55–62, doi:10.1016/j.memsci.2010.10.042

[24] M. Sahimi, *Flow and Transport in Porous Media and Fractured Rock*, Second, Revised and Enlarged Edition, WILEY-VCH Verlag GmbH & Co. KGaA, 2011, Weinheim, Germany